Detailed Atomistic Simulation of a Polymer Melt/Solid Interface: Structure, Density, and Conformation of a Thin Film of Polyethylene Melt Adsorbed on Graphite

Kostas Ch. Daoulas, Vagelis A. Harmandaris, and Vlasis G. Mavrantzas*

Department of Chemical Engineering, University of Patras, GR 26504, Patras, Greece, and Institute of Chemical Engineering and High-Temperature Chemical Processes (FORTH-ICE/HT), GR 26504, Patras, Greece

Received January 27, 2005; Revised Manuscript Received April 8, 2005

ABSTRACT: An atomistic modeling approach is presented for simulating the interface between a polymer melt and a crystalline solid substrate. As a test case, a thin film of polyethylene (PE) melt confined between a semiinfinite graphite phase on the one side and vacuum on the other is considered. The simulation is carried out in the NPT statistical ensemble with an efficient Monte Carlo (MC) algorithm based on state-of-the-art variable connectivity moves. The atomistic simulations are conducted by describing the PE chains with a united atom model, which considers each methylene (CH_2) and methyl (CH_3) group along the chain backbone as single interaction sites. To calculate the potential energy of interaction between polymer atoms and the semiinfinite graphite substrate, the method designed by Steele was implemented, capable of incorporating the exact crystallographic structure of graphite. The new approach has allowed us to analyze structural and conformational properties on the length scale of just a few angstroms from both surfaces. Detailed results are presented for the local mass density, structure, and conformation of PE at the two interfaces, obtained from simulations with model, strictly monodisperse PE samples of molecular length up to C_{400}. Additional structural features of the adsorbed layer, such as the distribution of skeletal carbon atoms in train, loop, and tail conformations and their statistics, are also analyzed in detail and compared with the predictions of the lattice-based Scheutjens−Fleer self-consistent mean-field theory in the limit of zero solvent concentration (melt case). Our atomistic simulation data demonstrate a stronger dependence of these descriptors of adsorbed layer structure on chain length than what is calculated by the mesoscopic Scheutjens−Fleer lattice model. In a second step, thoroughly equilibrated configurations of the confined model PE melt films are subjected to detailed molecular dynamics (MD) simulations in the NPT ensemble to analyze their dynamic behavior. The MD simulations are carried out with the rRESPA multiple-time-step algorithm and have allowed us to monitor segmental and chain center-of-mass mean-square displacements over time scales on the order of a few hundreds of nanoseconds. Results from the MD simulations are presented in the companion paper.

I. Introduction

In this two-part paper we discuss a computer modeling approach for studying the details of microscopic structural, conformational, thermodynamic, and dynamic properties of a polymeric liquid in the vicinity of an interface, under equilibrium conditions. We are concerned with a bulk multichain melt system, as opposed to a polymer solution, and its properties at the polymer/solid and polymer/vacuum interfaces. As an example, the interfaces between a polyethylene (PE) melt and a graphite basal plane on the one side and vacuum on the other are investigated. Our interest is in the development of a computer simulation method that can provide information not only on structural but also on dynamic characteristics of the melt at the two interfaces.

The motivation stems from the importance of polymer melt/solid and polymer melt/vacuum interfaces in a variety of applications involving adhesives, coatings, lubricants, and composite materials, where adsorbed molecules control the overall performance of the multiphase material system.[1−3] Polymer melt/solid interfaces, in particular, play a key role in applications involving polymer/polymer composites and polymer/particle nanocomposites, since the strength of chain attachment at interfaces (a quantitative thermodynamic measure of which is the work of adhesion)[1,2] governs the mechanical properties of the structure. They are also connected with sharkskin or melt-fracture phenomena such as those observed in polymer melt processing operations at high flow throughputs.[4] Even if the failure is not adhesive but cohesive (i.e., it starts at the bulk of the material), it may still be affected by the presence of the interface. This happens because of entropic constraints (chains cannot penetrate the solid boundary) and adsorption energy effects that cause significant deviations in the organization, shape, and density of the material relative to the bulk, unconstrained system. The length scale over which such changes take place and their extent govern all macroscopic properties of the multiphase system, so their knowledge is absolutely necessary in designing materials with optimal wetting and mechanical properties.

In distinct contrast to immiscible polymer/polymer interfaces, polymer free surfaces, and polymer solutions in the vicinity of an adsorbing solid surface which have been studied extensively in the past decades,[5−14] theoretical studies of polymer melt/solid interfaces have been rather sparse. From the point of view of applications, this is rather surprising since polymer melt/solid interfaces are the most interesting ones, being widely encountered in all polymer fluid flow processing opera-

* To whom correspondence should be addressed at the University of Patras: e-mail vlasis@chemeng.upatras.gr, tel (+30)-2610-997 398; fax (+30)-2610-965 223.

10.1021/ma050176r CCC: $30.25
Published on Web 06/01/2005

tions. Polymer melt surfaces and polymer melt/solid interfaces have extensively been investigated by Theodorou[15] through a variable density lattice model combining ideas from the Scheutjens−Fleer statistical theory for homopolymer adsorption[3] and the Sanchez−Lacombe equation-of-state theory.[16,17] The model was designed to predict surface thermodynamic and structural properties at the molecular level, based on parameters determined independently from the volumetric properties of the melt in the bulk.

The equilibrium structure and the dynamic behavior of a dense multichain system in the vicinity of walls were further studied by Mansfield and Theodorou[18] through dynamic MC simulations with relatively short chains, in the following cases: (a) a highly adsorptive surface with strong intersite potential barriers, (b) a highly adsorptive surface with no potential barriers, and (c) a weakly adsorptive surface with weak intersite barriers. Mansfield and Theodorou[19−21] developed computer simulation techniques to study also (a) the surface of a glassy atactic polypropylene (a-PP) exposed to vacuum and (b) the interface between bulk glassy a-PP and a graphite basal plane.

Bareman et al.[22] carried out MD simulations for systems of long-chain alkanes supported by a planar substrate and confined to surface densities appropriate to lipid and fatty acid monolayers at the air−water interface. Results were obtained for the density distribution normal to the surface, the structure factor parallel to the surface, and the number of chain conformational defects as a function of surface area per chain. MD was also employed by Xia et al.[23] to calculate segmental density profiles of *n*-hexadecane films of thicknesses ∼10, 20, and 40 Å adsorbed on a crystalline substrate [modeling Au(001)] at 350 K. The solid-to-liquid interface was characterized by a regularly spaced oscillatory profile of the film segmental density, with the amplitude of the density oscillations decreasing with increasing distance from the solid surface and extending up to 18 Å into the film.

Additional simulation studies of macromolecular liquids near solid surfaces have addressed issues related to the structure of polymer melts confined between two impenetrable plates with off-lattice MC[24] or stochastic dynamics simulations,[25,26] the wetting behavior of thin polymer films,[27−29] the melting behavior of *n*-alkane monolayers,[30] and aspects of structural relaxation and dynamic heterogeneity in a polymer melt at flat and structured surfaces.[31] These studies have been extended recently to the interaction of polymers with metal surfaces (such as that of liquid polycarbonate near a nickel surface)[32,33] by combining ab initio calculations (describing the interaction of fragments of the polymer with the surface) with molecular-level dynamic methods based on bead−spring models parametrized from the quantum chemical calculations.[32,33]

The quick literature survey proves that, despite the quite large number of simulation efforts, the model system has been typically a low molecular weight analogue of PE, of molecular length less than C_{60} if the simulation is carried out in full atomistic detail or less than 30 beads if the simulation is carried out with a coarse-grained, bead−spring model. The reason for this should be sought in the difficulties associated with the simulation of chain systems relative to either atoms or short polyatomic molecules as a result of the wide spectrum of time and length scales characterizing their dynamics and structure. The computational difficulties are more acute for the dynamic methods, such as MD, which are plagued by the problem of long relaxation times[34] that limits the simulation to times under a few hundreds of nanoseconds for MD simulations in the bulk and to times under 16 ns for MD simulations at interfaces.[31]

In this direction, MC methods can play a key role: through the design of clever (sometimes "unphysical", from the point of view of true dynamics) moves for generating new, trial configurations, they can accelerate system equilibration by many orders of magnitude more efficiently than MD, for the same model of molecular geometry and interatomic potential. It is the objective of the present work to extend existing studies of adsorbed polymer melts to higher chain length (up to C_{400}) systems and longer times (up to 100 ns), through the implementation of an efficient simulation methodology that employs robust MC algorithms to preequilibrate the system and analyze their static (thermodynamic and conformational) properties, and execution of long MD simulation runs with a multiple time step algorithm to get at their dynamic properties.[34] In the last years, such a methodology has been followed with remarkable success in order to simulate the structural and equilibrium dynamic properties of a number of long-chain polymers in the bulk;[34−38] it is extended here to interfacial systems in an effort to shed light on the mechanisms governing structure and dynamics in films of polymer melts adsorbed on a structured surface. As a test case, a thin film of PE melt supported by graphite on the one side and exposed to vacuum on the other is considered.

Key features of our approach are (a) the generation of realistic atomistic configurations, representative of the true polymer structure on the computer, thoroughly preequilibrated at the temperature and pressure conditions of the experiment with an efficient variable-connectivity MC algorithm, (b) the execution of long MC and MD simulations with appropriate intra- and interatomic interaction potentials representing as faithfully as possible the interactions in the real system under examination, and (c) the analysis of microscopic structural (such as density distribution, torsion angle distribution, chain shape, and bond orientation) and conformational features (distribution of adsorbed segments in tails, trains, and loops, and their statistics) and of the dynamic properties (segmental and chain center-of-mass mobility and their anisotropy) at the two interfaces down to the atomic level (smallest length scale equal to 1.54 Å). In all cases, the results of our interfacial simulations are compared to those of simulations with the corresponding unconstrained PE liquid carried out in the absence of the solid and vacuum surfaces. This part of the paper addresses details of local melt density, structure, and conformation of the melt at the two interfaces. The companion part addresses dynamic aspects of the confined film.

The remainder of the paper is organized as follows. Section II presents the molecular model for the PE melt and graphite substrate employed in our MC and MD simulations. Section III describes the simulated systems and our simulation strategy. Results from the atomistic MD and MC simulations for the density, structure, conformation, and chain organization in the adsorbed films are presented in section IV. Our findings and conclusions are summarized in section V.

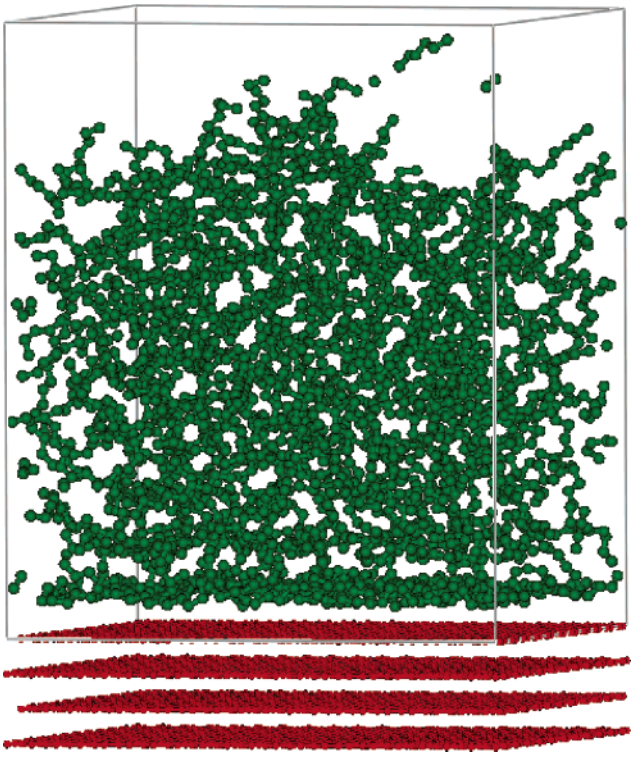

Figure 1. Model structure of a thin PE melt film confined between a semiinfinite graphite phase on its one side (bottom) and vacuum on its other side (top). The structure has been obtained from the MC simulation with the C_{78} melt and is representative of a fully relaxed system configuration at $T = 450$ K. Periodic boundary conditions apply only in the x and y directions of the coordinate system, along which the dimensions of the simulation box have been chosen to be integer multiples of the corresponding dimensions of the graphite unit cell ($L_x = 49.2$ Å and $L_y = 46.87$ Å, here).

II. Molecular Model

The systems studied in this work are thin films of PE melt exposed to a graphite surface on one side (e.g., at the bottom) and to vacuum on the other (e.g., at the top), along the z direction of an xyz Cartesian coordinate system. A relaxed model microstate (snapshot) of the confined film is shown in Figure 1. The functional form of the inter- and intramolecular interaction potentials between polymer atoms employed in our simulation is discussed in detail below. It is an atomistic model in a united-atom representation, according to which each methylene (CH_2) and methyl (CH_3) group along a PE chain is regarded as a single Lennard-Jones (LJ) interacting site.

For all intramolecular interactions between sites separated by more than three bonds and all intermolecular interactions, a spherically truncated 6−12 Lennard-Jones (LJ) potential is used:

$$V_{NB}(r) = V_{LJ}(r)\,\Pi(R_c - r) = \begin{cases} 4\epsilon\left[\left(\frac{\sigma}{r}\right)^{12} - \left(\frac{\sigma}{r}\right)^{6}\right], & r \le R_c \\ 0, & r > R_c \end{cases} \quad (1)$$

R_c in eq 1 is the cutoff distance, set equal to 9.875 Å in all simulations of this work, ϵ the well depth of the potential, and σ the collision diameter of the potential, while $\Pi(R_c - r)$ denotes the unit pulse function: $\Pi(R_c - r) = 1$ if $r \le R_c$, and $\Pi(R_c - r) = 0$ if $r > R_c$. Values for ϵ and σ have been borrowed from the TRaPPE model[39] ($\epsilon = 0.0914$ kcal/mol, $\sigma = 3.95$ Å), and no explicit distinction is made between the CH_2 and CH_3 united atoms. To calculate the attractive tail contribution to the total polymer/polymer interatomic potential energy due to cutoff, a technique based on the work of Mansfield and Theodorou[20] was followed, accounting explicitly for the nonuniform density profile across the film; it is described in detail in Appendix A.

Because of the truncation of the LJ potential at R_c in eq 1, the corresponding force

$$F_{NB}(r) = -\frac{dV_{NB}(r)}{dr} = \begin{cases} \frac{24\epsilon}{r}\left[2\left(\frac{\sigma}{r}\right)^{12} - \left(\frac{\sigma}{r}\right)^{6}\right] + V_{LJ}(R_c)\,\delta(r - R_c), & r \le R_c \\ 0, & r > R_c \end{cases} \quad (2)$$

exhibits a discontinuity at R_c, expressed by the term $V_{LJ}(R_c)\,\delta(r - R_c)$ involving the delta function $\delta(r - R_c)$.[40] The delta function is quite inconvenient to deal with in the MD simulation; on the other hand, failure to properly account for it can lead to significant errors, particularly in simulations of interfacial systems where relatively abrupt changes in the local mass density are present. In our work, the δ-term was handled by following the approximation proposed by Trokhymchuk and Alejandre:[40]

$$\delta(r - R_c) \to \frac{\Pi(r - R_c) - \Pi(r - R_c - \Delta r)}{\Delta r}, \quad \text{as } \Delta r \to 0 \quad (3)$$

where Δr is a fixed parameter chosen sufficiently small (equal to $\Delta r = 0.01\sigma$ here) so as not to influence the simulation results.

As far as the rest of the polymer/polymer interactions in the film is concerned, bond lengths l are kept constant in the simulations at their average value of 1.54 Å, while bond angles θ are assumed to fluctuate around an equilibrium angle $\theta_0 = 114°$ subject to the van der Ploeg and Berendsen harmonic potential:[41]

$$V_{bending}(\theta) = \frac{1}{2}k_\theta\,(\theta - \theta_0)^2 \quad (4)$$

with $k_\theta = 124.19$ kcal mol^{-1} rad^{-2}. Also, all dihedral angles ϕ are governed by a torsional potential of the form[42]

$$V_{torsional}(\phi) = \sum_{i=0}^{8} c_i \cos^i \phi \quad (5)$$

with $c_0 = 1.9887$, $c_1 = 4.2292$, $c_2 = -0.6018$, $c_3 = -7.1739$, $c_4 = 4.5024$, $c_5 = 3.9043$, $c_6 = -8.9158$, $c_7 = -3.4481$, and $c_8 = 5.5952$ in kcal/mol.

To calculate the potential energy of interaction between polymer atoms and the semiinfinite graphite substrate, the method designed by Steele[43] was implemented. According to this, the graphite phase is represented as a set of LJ carbon atoms centered at their crystallographically correct positions, while the solid structure is assumed to remain unperturbed by the adsorption of polymer. Taking advantage of the symmetry in the crystalline substrate, the potential energy of interaction between a polymer atom and the semiin-

finite graphite phase at distance r is written as

$$V_{\text{graphic}}(r) = V_0(r) + V_n(r) \tag{6a}$$

where V_0 and V_n are given through

$$V_0(r) = \frac{4\pi{\sigma_{\text{ps}}}^2\epsilon_{\text{ps}}}{\alpha_{\text{s}}}\sum_{a=0}^{\infty}\left[\frac{2}{5}\left(\frac{\sigma_{\text{ps}}}{z+ad}\right)^{10} - \left(\frac{\sigma_{\text{ps}}}{z+ad}\right)^{4}\right]$$

$$V_n(r) = \frac{2\pi{\sigma_{\text{ps}}}^6\epsilon_{\text{ps}}}{\alpha_{\text{s}}}\sum_{n>0}^{5}\left[\frac{{\sigma_{\text{ps}}}^6}{30}\left(\frac{g_n}{2z}\right)^5 K_5(g_n z) - 2\left(\frac{g_n}{2z}\right)^2 K_2(g_n z)\right] f_n(s_1,s_2) \tag{6b}$$

In eqs 6, σ_{ps} and ϵ_{ps} are the values of the collision diameter and well depth, respectively, of the LJ potential describing the pair interaction between a polymer united atom and a graphite atom (calculated using the Lorentz−Berthelot rule), α_{s} the area of the surface unit cell, d the distance between successive graphite basal planes, g_n numerical coefficients, K_2 and K_5 modified Bessel functions of the second kind, and s_1 and s_2 parameters defining the x and y coordinates of the projection of the polymer atom on the first graphite basal layer ($z = 0$) relative to the surface unit cell; they range from 0 to 1. Values for the coefficients g_n and the functions $f_n(s_1,s_2)$ can be found in the original work of Steele.[43] The 10−4 sum is performed explicitly[20] over the first 63 underlying layers of graphite atoms; for the rest of the layers, the interaction is accounted for by smearing graphite carbons in all three directions, resulting in a 9−3 potential for $V_0(z)$ of the form:

$$V_0(z) = \frac{4\pi{\sigma_{\text{ps}}}^2\epsilon_{\text{ps}}}{a_{\text{s}}}\sum_{a=0}^{63}\left[\frac{2}{5}\left(\frac{\sigma_{\text{ps}}}{z+ad}\right)^{10} - \left(\frac{\sigma_{\text{ps}}}{z+ad}\right)^{4}\right] + \frac{4\pi{\sigma_{\text{ps}}}^2\epsilon_{\text{ps}}}{3a_{\text{s}}d}\left[\frac{2}{15}\left(\frac{\sigma_{\text{ps}}}{z+64d}\right)^{9} - \left(\frac{\sigma_{\text{ps}}}{z+64d}\right)^{3}\right] \tag{6c}$$

III. Systems Studied and Simulation Strategy

With the molecular model described in section II, detailed atomistic MC and MD simulations were performed with model linear, strictly monodisperse PE melt samples. The simulation box was always orthorhombic with different edge lengths, L_x, L_y, and L_z, along the x, y, and z directions of the coordinate system. Periodic boundary conditions were applied only along x and y, meaning that we are simulating an infinite system there; in contrast, a finite film thickness was assumed along the z direction. L_x and L_y were chosen to be commensurate with the periodicity of the graphite substrate along x and y, respectively, while L_z was taken to be considerably larger than the thickness of the adsorbed polymer film, L_z^{film}, at equilibrium. For all simulated molecular lengths, the latter was chosen to be at least 3 times larger than the equilibrium root-mean-square radius-of-gyration of a PE chain in the bulk, R_g. To prevent chains from exiting the simulation box in the z direction, a "soft wall" was placed at the upper face of the orthorhombic cell.[19]

The following systems were simulated in this work: a 80-chain C_{40}/graphite melt, with $L_x = 49.2$ Å, $L_y = 46.87$ Å, and $L_z^{\text{film}} \sim 46$ Å; a 50-chain C_{78}/graphite melt, with $L_x = 49.2$ Å, $L_y = 46.87$ Å, and $L_z^{\text{film}} \sim 54$ Å; a 48-chain C_{156}/graphite melt, with $L_x = 59.04$ Å, $L_y = 59.65$ Å, and $L_z^{\text{film}} \sim 66$ Å; a 48-chain C_{250}/graphite melt, with $L_x = 68.88$ Å, $L_y = 68.17$ Å, and $L_z^{\text{film}} \sim 79$ Å; and a 48-chain C_{400}/graphite melt, with $L_x = 68.88$ Å, $L_y = 68.17$ Å, and $L_z^{\text{film}} \sim 125$ Å.

Our simulation strategy involved the following steps: (i) Generation of an initial configuration for the film under study through a "biased" pseudo-MC approach,[44] which builds up each chain in the simulation box atom-by-atom by avoiding significant intra- and intermolecular mer−mer overlaps, as well as overlaps with the solid barrier. (ii) Minimization of the total potential energy of the initial structure with respect to all microscopic degrees of freedom, through a modified version of the amorphous cell method of Theodorou and Suter[44] accounting for the presence of the graphite substrate and vacuum. (ii) Thermal equilibration of the generated minimum potential energy system microstructure with an atomistic MC simulation in the isothermal−isobaric (NPT) statistical ensemble, at $T = 450$ K and $P = 0$ atm. (iv) Execution of a long atomistic MD simulation with the resulting relaxed configurations in the isothermal−isobaric (NPT) statistical ensemble, at $T = 450$ K and $P = 0$ atm, for times up to 100 ns.

The MC simulations have been carried out with our variable connectivity algorithm.[35−38] Built around a set of simple, such as reptation, flip, and end-mer rotation, but also more complex, mostly "unphysical" moves, such as concerted rotation, end-bridging (EB), self-end-bridging (SEB), double bridging (DB), and intramolecular double rebridging (IDR), this very efficient algorithm has developed to a principal research tool for simulating chain systems of a variety of chemical constitution and architectures.[35,36] Polyolefin and polydiene melts, oriented systems, binary systems composed of chemically similar macromolecules, and polymers terminally grafted to a substrate have all been simulated with this MC algorithm in continuous space and full atomistic detail. To keep the simulated systems strictly monodisperse, the MC simulations of the present work were carried out with the following (typical) mix of moves: 5% rotations, 5% flips, 10% configurational bias moves, 25% concerted rotations, 7% reptations, 30% double-bridgings, and 18% intramolecular double rebridgings.

The MC method cannot, unfortunately, provide any direct dynamic information. Because of its dynamical nature, MD remains the only molecular simulation method that can give real-time information for the evolution of an atomistic system. MC can, however, facilitate the calculation of the dynamic properties through MD by providing the initial, thoroughly equilibrated at all length scales, model configurations; a similar strategy was also followed here. The MD simulations were executed by employing the velocity Verlet method[45] for the integration of the equations of motion, with all C−C bond lengths being kept fixed in the course of the simulation at their equilibrium values through an efficient implementation of the SHAKE method.[46,47] A multiple time step (MTS) algorithm (the rRESPA method) was employed for the force calculations.[48] According to this, the *faster* degrees of freedom in the system are integrated with a *small* time step, dt, while the *slower* ones are integrated with a *larger* time step, Dt. In the present MD simulations $dt = 1$ fs and $Dt =$

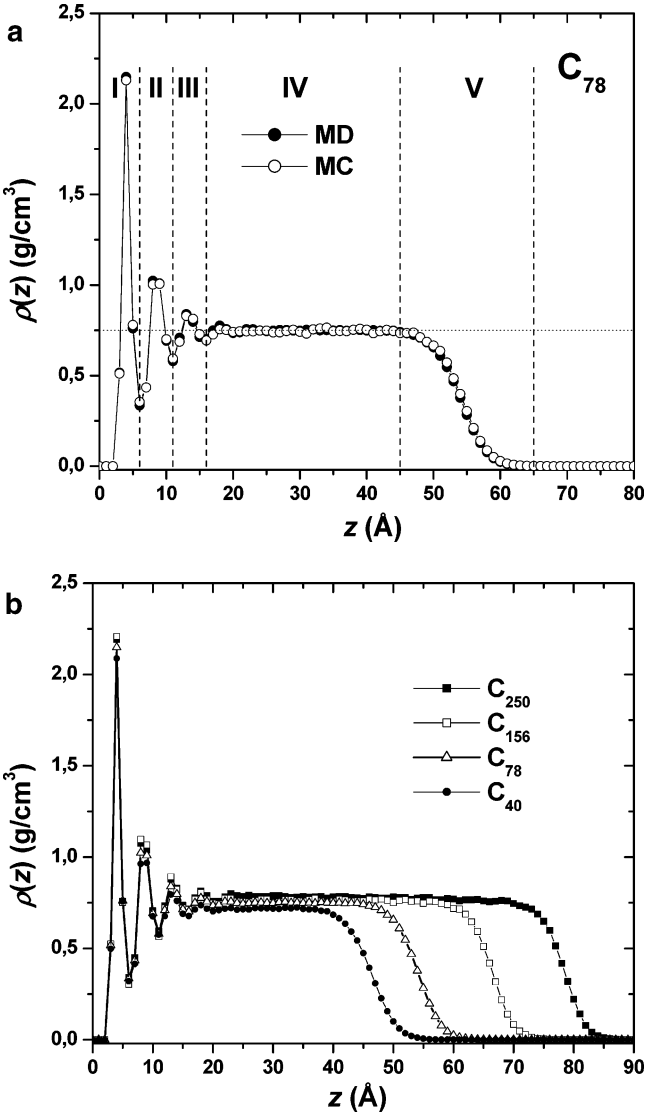

Figure 2. (a) Local mass density distribution across the C_{78} PE film, as obtained with the double-bridging MC and rRESPA MD algorithms. The vertical dashed lines serve as eye guides and are used to define the borders of the five regions in which space is divided in the film to facilitate the analysis of structural and conformational properties. The horizontal dotted line denotes the density value of a bulk C_{78} melt. (b) Local mass density distributions for all simulated systems [$T = 450$ K].

2 fs. The overall simulation time of the MD runs varied from 20 up to 100 ns depending on the molecular length and size (total number of atoms) of the simulated system.

IV. Results

Melt Structure. How chains organize in the two interfacial regions has been analyzed by dividing space across the film into bins separated by planes parallel to the solid surface, of width equal to 1 Å. Within each bin, values of characteristic structural and conformational properties for each system were obtained by averaging over all configurations accumulated in the course of the MC or MD run. Figure 2a displays the mass density distribution, $\rho(z)$, across the film for the C_{78} system, as obtained separately from the MD and MC simulations. The two curves are identical, proving the consistency of the two simulation algorithms. Near the graphite, the density profile exhibits a characteristic oscillatory behavior wherein three at least peaks can be discerned, at distances equal to 4, 8.5, and 13 Å from the graphite plane; a fourth peak at 18 Å is also discerned, but with a considerably smaller height. The first peak, just 4 Å from the highly attractive graphite surface, is the strongest; it appears at a distance roughly equal to the sum of the van der Waals radii of the CH_2 groups and graphite carbons. Similar density profiles with the characteristic oscillatory features have been observed in past simulations of polymer/solid interfaces with either coarse-grained bead−spring[49] or atomistic models.[23,31] In the middle region of the film, at distances beyond 20 Å from graphite, $\rho(z)$ attains a constant value equal to the density of the free (unconstrained) C_{78} PE melt at $T = 450$ K (0.75 g/cm^3). On the other hand, at the polymer/vacuum interface the melt density gradually drops to zero, exhibiting the characteristic sigmoidal shape typical of a melt free surface.[15]

The profile of the local mass density distribution shown in Figure 2a is typical of all PE melts (C_{40}, C_{78}, C_{156}, C_{250}, and C_{400}) simulated here; this is demonstrated in Figure 2b. According to Figure 2b, the characteristic distances at which the adsorption peaks appear are equal in all systems, independently of their molecular length. It is also observed that, as the chain length of the melt increases, the bulk value of the density in the middle regions of the film increases in exactly the same way as in a bulk PE melt.[37,38] However, with increasing chain length, the local mass density at the polymer/vacuum interface drops to zero more steeply; i.e., the width of the melt/vacuum interface decreases with increasing chain length. This is known in the literature and is connected to the increase in the surface tension of the melt with increasing polymer molecular weight.[15,50]

Further information on the structural features of the PE/graphite and PE/vacuum interfaces and the degree of deviation from bulk characteristics can be obtained by analyzing the spatial distribution of segments at the two interfaces as a function of their ranking number along the chain backbone. The local density at distance z above the surface, $\rho(z)$, can be considered as the sum of contributions $\rho_i(z)$ from all ith atoms along the chain, $i = 1, 2, ..., N$, where N is the chain length. For the free melt, $\rho_i(z) = \rho_b/N$, where ρ_b denotes the bulk melt density, since all atoms contribute equally (they are equivalent) to the total mass density. Consequently, the degree to which the ratio $\rho_i(z)/(\rho_b/N)$ departs from one is a measure of the extent to which the contribution of the ith segment to the local mass density departs from that in the corresponding free melt:[15] $\rho_i(z)/(\rho(z)/N)$ values greater (or less) than one will indicate an enhancement (or depletion) of the area at distance z from the boundary in ith segments. Figure 3 shows $\rho_i(z)/(\rho(z)/N)$ profiles for the first and last methyl groups (ends) along a PE chain and for the middle atoms, as obtained from our MD simulations with the C_{78} system (identical results are obtained with the MC algorithm). The strong tendency of chain ends to preferentially concentrate at the attenuated, "free" surface region of the PE/vacuum interface is clear in the figure; no such strong preference is observed in the PE/graphite interface. On the other hand, the contribution of inner atoms to the local mass density is more uniform across the film: despite their little preference to lie next to graphite as opposed to free surface, the deviation of their distribution from the bulk uniform profile is not appreciable.

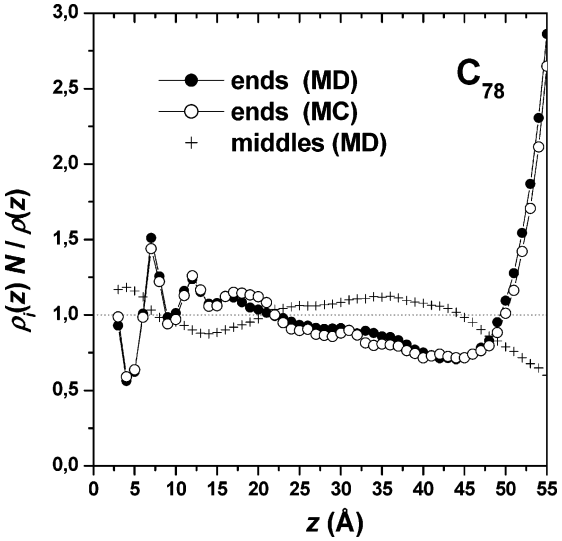

Figure 3. Chain end density profile normalized with its bulk value from our MD (solid circles) and MC (open circles) simulations with the C_{78} PE melt system at $T = 450$ K. Crosses show the corresponding distribution of the middle carbon atoms along the chain, as derived from MD.

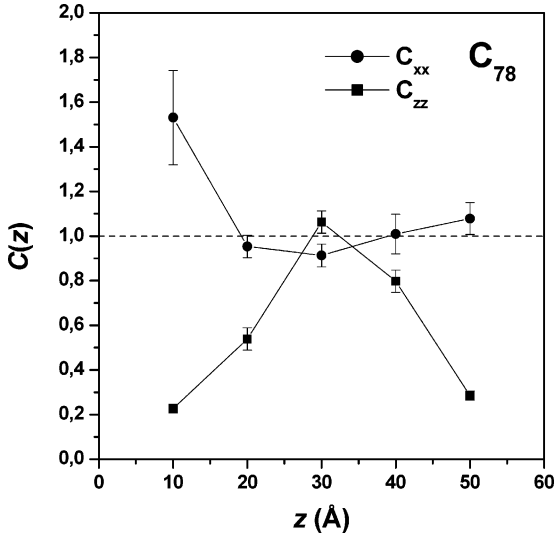

Figure 4. C_{xx} (filled squares) and C_{zz} (filled circles) components of the conformation tensor **C**, as a function of the distance of the chain center of mass from the solid substrate. The results have been obtained from the MC simulation with the C_{78} melt at $T = 450$ K.

Overall Melt Conformation. Changes in the shape of the chains can be analyzed in terms of a global descriptor of the overall polymer melt configuration, the so-called conformation tensor **C**. This is defined as the second moment tensor of the end-to-end distance vector, **R**, of a polymer chain reduced by one-third its unperturbed mean-square end-to-end distance, $\langle R^2 \rangle_0$, averaged over all chains in the system:

$$\mathbf{C} = 3\left\langle \frac{\mathbf{RR}}{\langle R_0^{\,2} \rangle} \right\rangle \tag{7}$$

Away from any boundary, chain conformational statistics is unperturbed, to an excellent approximation; therefore, **C** reduces to the unit tensor, $\mathbf{C} = \mathbf{I}$. When the melt is subjected to a flow field over time scales shorter than or comparable to the longest relaxation time of the chains, or when the melt is found in the neighborhood of a boundary, chain shapes are distorted and **C** departs from its equilibrium isotropic value. In such a case, the nonzero components of **C** provide a measure of the orientation and/or extension of the chains along the three axes of the coordinate system.

Figure 4 displays the effect of the graphite phase on the C_{xx} and C_{zz} components of the conformation tensor **C** parallel and perpendicular to the plane, respectively. The results have been obtained from the MD simulation with the C_{78} PE melt. [The C_{yy} component is not shown since, on the average, $C_{yy} = C_{xx}$ due to ellipsoidal symmetry.] Five pairs of data are shown in each part of the figure, corresponding to C_{xx} and C_{zz} values obtained by analyzing chain conformations separately after dividing space across the film in 10 Å thick layers. Within each layer, **C** is obtained as an ensemble average of individual molecular conformation tensors over chains whose centers-of-mass lie in that layer. The first two layers are representative of the topology and structure of the system near the graphite phase, the third of the middle region of the film where density assumes bulk-like characteristics, and the fourth and fifth ones correspond to the structure and topology of the melt free surface. It is demonstrated that chain conformations across the film depart significantly from their bulk shape. Chains with centers-of-mass closest to the graphite phase (region I in Figure 2a) are characterized by very small C_{zz} ($= 0.20 \pm 0.05$) and relatively large C_{xx} ($= C_{yy} = 1.50 \pm 0.20$) values, indicative of a conformation that is compressed along the z and elongated along the x and y directions of the coordinate system. Consequently, chains right next to the adsorbing graphite surface are very narrow, lying practically flat on the plane. Chains are found to be flattened also in the next layer (region II in Figure 2a) but to a lesser degree: $C_{zz} = 0.50 \pm 0.10$ and $C_{xx} = C_{yy} = 0.95 \pm 0.10$ there. Deeper in the fluid phase (region III in Figure 2a), the flattening disappears, and chain conformations become representative of a bulk system: $C_{xx} = C_{yy} = 1.10 \pm 0.10$ and $C_{zz} = 0.90 \pm 0.10$ there. Chains appear to be quite flattened also in the highly attenuated free surface region, indicative of their tendency to lie parallel to the free surface of the melt due to cohesive forces: $C_{xx} = C_{yy} = 0.80 \pm 0.10$ and $C_{zz} = 1.00 \pm 0.05$ in region IV (see Figure 2a), while $C_{xx} = C_{yy} = 1.10 \pm 0.10$ and $C_{zz} = 0.30 \pm 0.10$ in region V (see Figure 2a).

On the basis of the results of Figure 4, for the C_{78} melt studied here, the length scale over which the transition to bulk polymer characteristics takes place is approximately 30 Å from the graphite phase as far as the perpendicular component, C_{zz}, of the conformation tensor, **C,** is concerned but only 20 Å as far as its two parallel components, C_{xx} and C_{yy}, are concerned; these distances are equal to 2.1 and 1.4 times the equilibrium (bulk) mean radius of gyration, R_g, of the C_{78} PE melt. On the other hand, if one focuses on the free surface of the melt, the distance beyond which chain conformations attain their bulk characteristics is practically the same for all three diagonal components of the conformation tensor and approximately equal to 20 Å. In general, the two interfaces affect more the perpendicular (C_{zz}) rather than the two lateral components (C_{xx} or C_{yy}) of **C**, which agrees with recent experimental data[51] and earlier computer simulation studies.[20,52,53]

Local bond orientation tendencies induced by the two boundaries are also of interest. They can be discussed

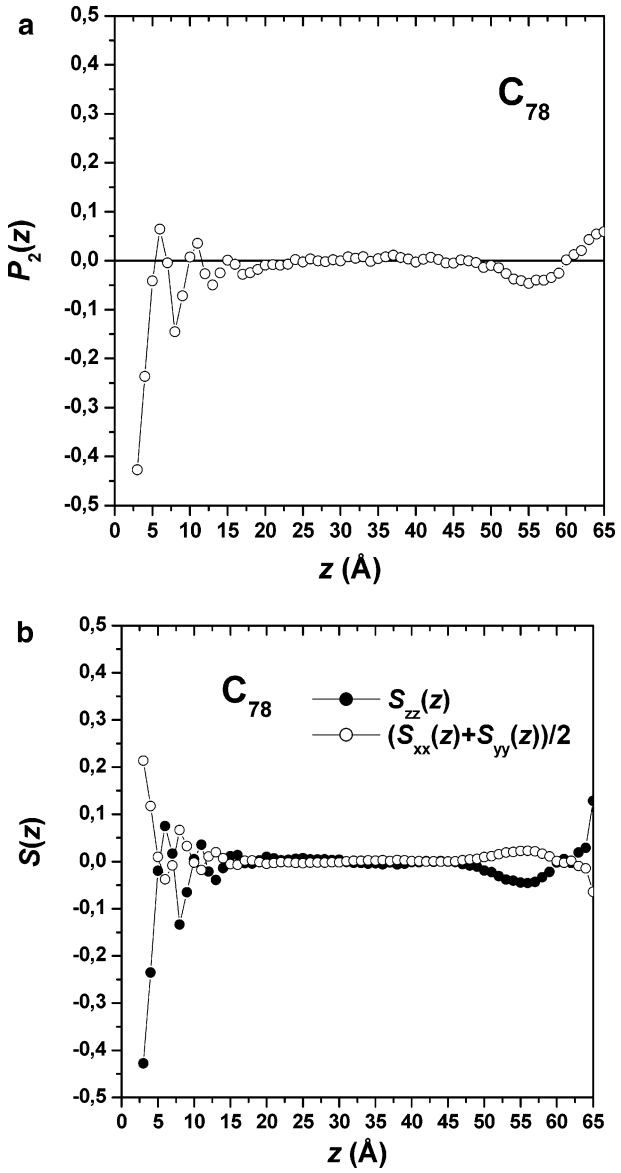

Figure 5. (a) Local order parameter, $\langle P_2(\cos\theta)\rangle$, for C−C bonds as a function of distance from the solid. (b) Values of the diagonal components of the Sauppe matrix, S_{ab}, as a function of distance, z, from the solid. The results have been obtained from the MC simulations with the C_{78} melt at T = 450 K.

in terms of the average C−C second rank bond order parameter, defined as

$$\langle P_2(\cos\theta)\rangle = \left(\frac{3}{2}\langle\cos\theta^2\rangle - \frac{1}{2}\right) \tag{8}$$

where θ is the angle formed between a C−C bond and the z coordinate axis (normal to the surface). Simulation results for the variation of $\langle P_2(\cos\theta)\rangle$ with bond distance from the graphite phase are presented in Figure 5a; they have been obtained from our MC simulations with the C_{78} system (identical results have been obtained from the MD simulation). The limiting values for $\langle P_2(\cos\theta)\rangle$ are −0.5, 0.0, and 1.0 for perfectly parallel, random, and perpendicular bond orientation relative to the planar surface, respectively. An oscillatory pattern is obtained in Figure 5a for the $\langle P_2(\cos\theta)\rangle$ parameter, resembling very much that of the local mass density distribution (see Figure 2a). Right next to the graphite plane, in particular, $\langle P_2(\cos\theta)\rangle$ attains large-in-magnitude, negative values (e.g., $\langle P_2(\cos\theta)\rangle \approx -0.4$ at $z = 3$ Å), indicative of the strong tendency for C−C bonds to orient parallel to the solid plane. [Here, we would like to draw the reader's attention to the united-atom nature of our atomistic model, in which the effect of pendant hydrogens on the C−C bond orientation is lost. Consequently, the present simulation data for the variation of the $\langle P_2(\cos\theta)\rangle$ C−C order parameter for distances less than about 6 Å from the graphite surface should be interpreted with extreme caution. The design of an all-atom model and its application in simulations with thin PE films such as those discussed here is the subject of work currently in progress.]

The characteristic oscillatory pattern of the $\langle P_2(\cos\theta)\rangle$ bond order parameter is evidenced up to distances 20 Å from the graphite phase. Beyond this, in the middle region of the film, $\langle P_2(\cos\theta)\rangle$ becomes zero, characteristic of a random C−C bond orientation. This behavior is observed up to distances just below the melt/vacuum interface. There, $\langle P_2(\cos\theta)\rangle$ assumes again nonzero values, but its variation with local position is not monotonic: it attains slightly negative values in the interval 50 Å $< z <$ 60 Å, manifesting a tendency for C−C bonds to lie parallel to the free surface of the polymer film due to cohesive forces, and becomes positive at the extreme region of the melt, manifesting a tendency for chain ends to stick out into the vacuum phase. These results are in full agreement with the predictions of Theodorou's lattice-based, variable density self-consistent-field model.[15] Similar profiles have been obtained from the present MC and MD simulations with the rest of the simulated PE samples.

To analyze the uniaxial (or not) character of the anisotropy exhibited by the C−C bonds, we have calculated all elements of the traceless, symmetric Saupe matrix, **S**:[54]

$$S_{ab} = {}^3/_2\langle l_a l_b\rangle - {}^1/_2\delta_{ab} \tag{9}$$

where l_a, $a = x, y, z$, are the direction cosines relating C−C bonds to the laboratory Cartesian coordinate frame. For phases characterized by uniaxial anisotropy (along, e.g., the z direction), all off-diagonal elements of the Saupe matrix should vanish while the diagonal ones should satisfy the condition: $S_{xx} = S_{yy} = -{}^1/_2 S_{zz}$. Simulation results for the diagonal elements of the Saupe matrix obtained from the MD simulation with the C_{78} system are reported in Figure 5b: within the statistical accuracy of the simulation data, the uniaxiality conditions are identically satisfied in the two interfacial zones.

Perturbations in the local PE chain conformation have further been analyzed in terms of deviations of the torsion angle distribution from the bulk pattern. Results obtained from the MD simulation with the C_{250} system are presented in Figure 6a. Separate torsion angle population curves are shown in the figure for regions I and IV of the films (see Figure 2a); the rest are omitted for clarity since they are practically identical to that reported for region IV. Except for region I where a nonnegligible enhancement of trans states is observed, the distribution in all other layers remains practically unaltered. This effect is further investigated in Figure 6b presenting the percentage of bonds in trans and gauche states as a function of local position. With the term trans here we mean all torsion angles with values

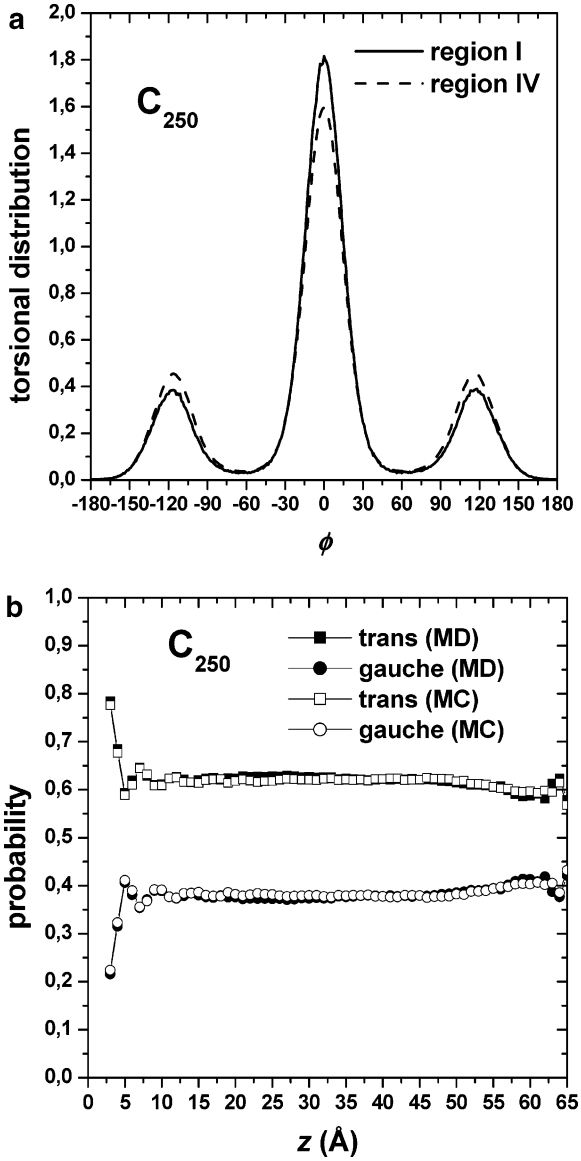

Figure 6. (a) Torsion angle distribution for the C_{250} PE system in regions I and IV of the film, as obtained from the MD algorithm at $T = 450$ K. (b) Trans and gauche state probabilities along the z axis for the C_{250} PE melt at $T = 450$ K, as obtained from the MD (filled symbols) and the MC (open symbols) simulations.

between −60° and +60°; angles with values outside this interval are considered as gauche. Right next to the graphite substrate ($z < 5$ Å), a significant increase in the trans population is observed, in agreement with other atomistic MD simulations.[25] In contrast, near the free surface of the melt, a strong enhancement of gauche conformations is observed; this is also in agreement with the predictions of the atomistic simulations of Mansfield and Theodorou for the free surface of glassy a-PP.[19] At distances beyond 15 Å from the graphite plane, or below 10 Å from the free surface, the relative population of torsional conformations in trans and gauche states is the same as in the bulk.

Adsorbed Melt Conformation. In this section we present a selection of simulation results referring to certain structural features of the adsorbed layer, such as the adsorbed amount, the distribution of individual carbon atoms in trains, loops, and tails, and their statistics; the dependence of these descriptors of the local structure of the films on chain length is also analyzed.

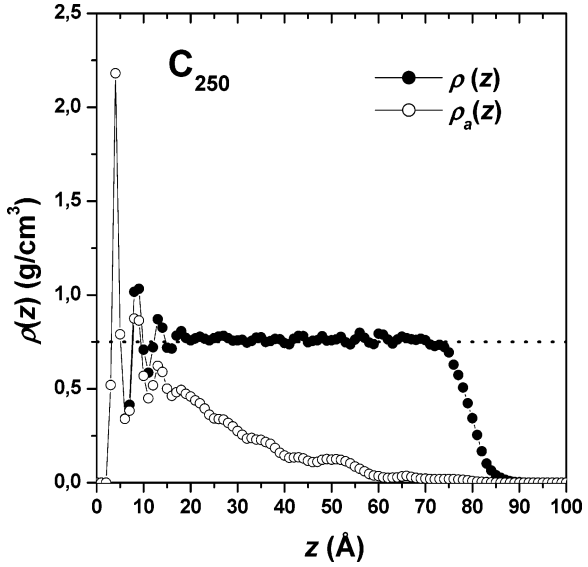

Figure 7. Contribution to the total mass density profile, locally, of adsorbed segments for the C_{250} PE melt. The results have been obtained with the MD simulation algorithm (identical results have been obtained with the MC algorithm) [$T = 450$ K].

Adsorbed Amount. Following Scheutjens and Fleer,[6] the adsorbed amount Γ is defined as the total mass of carbon atoms belonging to adsorbed chains per surface area unit. A chain is considered as adsorbed if it has at least one adsorbed carbon atom, i.e., one carbon atom that lies a distance less than 6 Å from the adsorbing graphite plane. This is the distance separating the first two maxima in the local mass density profile (see Figure 2a) and is considered to define the boundaries of the first adsorption layer (termed region I). A similar definition has been used in earlier variable density atomistic MD simulations of short (C_{13} and C_{28}) alkane melts above a solid substrate.[25] The profile of the resulting local mass density distribution of adsorbed segments, $\rho_a(z)$, is shown in Figure 7 (open circles); for comparison, we also show in the figure the total mass density profile (filled circles). The results have been obtained from the MC simulation with the C_{250} PE system. By definition, all carbon atoms found in the first adsorption layer are adsorbed; what Figure 7 shows then is that a considerable amount of polymer mass found in the second and third adsorption layers (70% for the former and 44% for the latter) belong to adsorbed chains. The rest of the polymer mass in these two layers is "free"; i.e., it belongs to chains that do not have any adsorbed segment. The local mass density of adsorbed segments decreases continuously with increasing distance from the graphite plane, before dropping to zero further away at a distance which is a strong function of the molecular weight of the adsorbed melt. As will be shown in the next paragraphs, the adsorbed segment density profile at larger distances is due to the presence of the long dangling tails.

The adsorbed amount Γ is obtained from Figure 7 by integrating the function $\rho_a(z)$; it is plotted on a log−log plot as a function of chain length in Figure 8. The two sets of data reported in Figure 8 have been independently obtained from the MC and MD simulation methods and coincide. By performing a linear regression analysis in the data, Γ is found to exhibit a power law

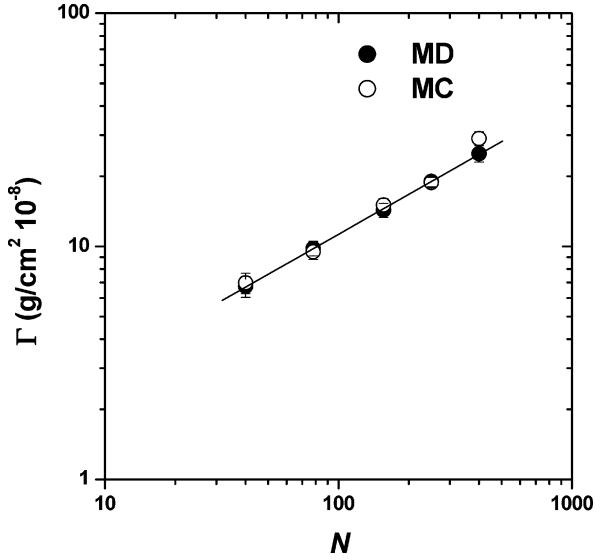

Figure 8. Adsorbed amount Γ as a function of chain length N, at $T = 450$ K. Two sets are shown in the figure, corresponding to the two different simulation algorithms with which the results have been obtained; the agreement is excellent.

dependence on chain length N of the form $\Gamma = A + BN^n$, with $n = 0.57 \pm 0.03$; the corresponding value reported by Scheutjens and Fleer[6] is $n = 0.50$. The main reason for the deviation should be sought in the relatively short chain length of the melts studied here: The Scheutjens–Fleer lattice-based prediction is reported to be valid for values $r > 100$, where r denotes the number of polymer "segments" along the chain. "Segments" can be understood in terms of either Flory or Kuhn statistical units.[55] The absence of any correlation between successive lattice polymer segments in the Scheutjens–Fleer model suggests that they had better be interpreted as Kuhn statistical units. Utilizing the data for the dependence of the characteristic ratio on chain length for linear PE melts,[38,56] the following values are obtained for the number of Kuhn statistical units r corresponding to the chain length N of our PE melts: $r = 3.8$ for the C_{40} chains, $r = 6.9$ for the C_{78} chains, $r = 13.3$ for the C_{156} chains, $r = 21.1$ for the C_{250} chains, and $r = 33.6$ for the C_{400} chains. These suggest that a segment in the Scheutjens–Fleer lattice model should correspond to roughly 12 carbon atoms in our atomistic model. We realize therefore that all PE melts studied here are too short compared to the regime of molecular lengths for which the scaling laws of the Scheutjens–Fleer theory are valid, and this may explain the discrepancy observed in the values of the exponent n quantifying the dependence of Γ on N. A second reason for the deviation is the neglect of compressibility effects in the Scheutjens–Fleer lattice statistical theory, particularly in the light of data shown in Figure 2a. Simulations with PE melts longer than C_{400} are needed to test the validity of the self-consistent mean-field theory of Scheutjens–Fleer more rigorously; results from such simulations will be presented in a future publication.

Statistics of Trains, Loops, and Tails. A more detailed picture of the structure of the adsorbed PE melt layer is obtained by analyzing the statistics of conformations formed by adsorbed segments in the interfacial area, namely trains, loops, and tails.[6] Consistently with the definition of adsorbed chains (see also Figure 9) (a) *trains* are defined as successive C–C bonds with centers inside the adsorbed layer, i.e., at a distance less than 6 Å from the graphite plane; (b) *loops* are defined as sequences of C–C bonds connecting two trains, with centers, however, outside the adsorbed layer; while (c) *tails* are defined as sequences of C–C bonds terminated at one side by a nonadsorbed chain end and at the other side by an atom connected to a train. In all cases, the *length*, s, of a train, loop, or tail conformation is defined as the number of C–C bonds forming that train, loop, or tail.

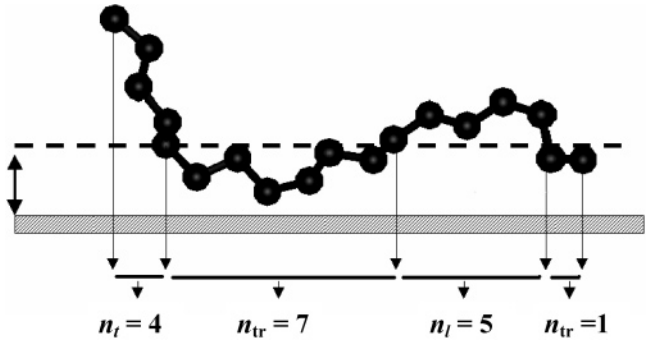

Figure 9. Schematic explaining the definitions of train, loop, and tail conformations of adsorbed chains.

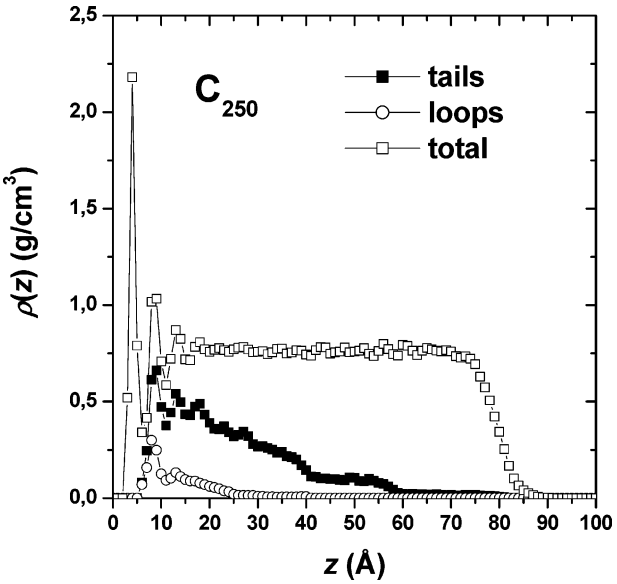

Figure 10. Tail (filled squares) and loop (open circles) contributions to the local mass density profile (open squares), for the C_{250} PE melt [$T = 450$ K].

With these definitions, the distribution of adsorbed carbon atoms has contributions from bonds belonging to trains, loops, and tails; these are denoted as $\rho_{tr}(z)$, $\rho_l(z)$, and $\rho_t(z)$, respectively. By convention, $\rho_{tr}(z)$ comprises all atoms belonging in the first adsorption layer, i.e., at distances less than 6 Å from the graphite plane. At distances greater than 6 Å, individual distributions of adsorbed segments are analyzed in terms of only $\rho_l(z)$ and $\rho_t(z)$. Figure 10 presents a typical plot of the local mass density profile and its tail and loop components, as a function of distance from the graphite surface. The results have been obtained from the MD simulation with the C_{250} PE melt (the MC simulation has given identical results). The figure shows that, except from a very narrow region from the graphite plane of thickness less than 7 Å, the local mass density profile is dominated by tails, which are observed to extend quite deeply in the liquid phase. It also shows that at around 10 Å the tail profile exhibits a maximum.

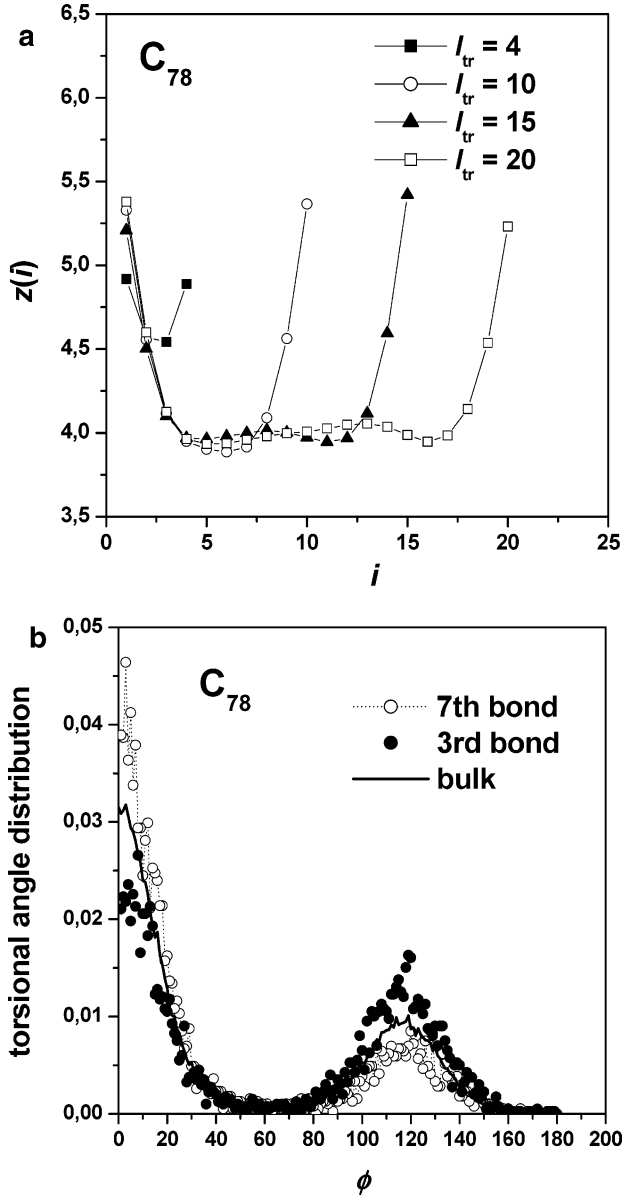

Figure 11. (a) Mean distance, $z_{tr}(i)$, from the graphite plane of the ith C−C bond of a train, as a function of rank number i and train size. (b) Torsion angle probabilities characterizing the distribution of the 3rd and 7th bonds along 15-mer long trains; due to symmetry, only half of the distribution is shown. For comparison, we also show the torsion angle distribution as obtained from a simulation with a bulk, unconstrained PE melt [$T = 450$ K].

As defined above, trains comprise segments belonging to the first adsorption layer. To analyze the train distribution, in Figure 11a we calculated the mean distance $\langle z_{tr}(i)\rangle$ above the graphite plane of the ith carbon atom along the train as a function of its ranking number i in the train and the train size. The function $\langle z_{tr}(i)\rangle$ has the meaning of a mean train trajectory along the z axis and for train lengths equal to 4, 10, 15, and 20 bonds is shown in Figure 11a. The results have been obtained from our MC simulation with the C_{78} system. Given the limitations in sampling a sufficient number of trains of a given size, the symmetry of all curves in Figure 11a with respect to the middle train segment is astonishing. On the average, all carbon atoms in the interior of a train are located at a distance equal to about 4.0 Å from the graphite plane (corresponding to the minimum of the graphite−polymer potential energy). They are bridged with other chain segments lying outside the first adsorption layer (i.e., at distances greater than 6 Å from the graphite plane) with just three bonds on either side of the train irrespective of the train size; these bonds have to "stick out" to reach carbon atoms belonging to the second adsorption layer.

Additional insight into the structure of trains can be gained by inspecting their torsional characteristics. This is demonstrated in Figure 11b presenting the torsion angle distribution of the two kinds of population making up a train: interior bonds and penultimate bonds. The results have been obtained from the MD simulation with the C_{78} melt by analyzing 15 bond-long trains (identical plots are obtained from the MC simulations with the same system). To reduce the statistical noise, the symmetry of the torsion angle distribution with respect to $\phi = 0$ was invoked; thus, in Figure 11b, only the distribution for angles ϕ in the interval [0,180] is shown. To compare against the statistics of the unconstrained melt, also shown in the figure (by the solid line) is the torsion angle distribution for a bulk (unperturbed) C_{78} PE melt. The preponderance of the adsorbed interior train bonds to form sequences of all-trans conformations along the graphite plane on which they prefer lying flattened is clear in the figure. In contrast, penultimate or bridging atoms form sequences that retain an increased population of gauche angles.

The distribution of torsion angles in train conformations and the profile of the mean train trajectory provided by Figure 11a allow one to explain the silent features accompanying abrupt alterations in the distribution of torsion angles between trans and gauche states that take place at short distances above the graphite phase (see also Figure 6b). The maxima observed in the trans population at approximately 4, 8, and 13 Å correspond to the three adsorption layers wherein C−C bonds tend to orient parallel to the graphite surface. The gradual decrease in the trans population (which is accompanied by a slight increase in the gauche states) observed in valleys of reduced mass density (at about 6 and 10 Å from the graphite plane) is due to the penultimate C−C bonds bridging carbon atoms located in successive (i.e., adjacent) adsorption layers.

In Figure 12a, we consider the train size distribution as a function of chain length. What is shown in the figure is the fraction of trains of length s, $P_{tr}(s) = n_{tr}(s)/n_{tr}$, and its dependence on chain length. For all chain length systems studied, $P_{tr}(s)$ follows a nonmonotonic behavior with s. Starting from a relatively high value at very short train sizes ($s = 1$ and 2), $P_{tr}(s)$ goes through a sharp minimum for a train size equal to 4 or 5 bonds, and then it steeply rises up to go through a maximum for a size $s = 7$, after which it monotonically decreases to zero for high enough sizes. This behavior is observed for all PE melts studied except the shorter (alkane-like) C_{40}, C_{60}, and C_{78} melts for which an exceptionally large number of trains of size $s = 39$, 59, and 77, respectively, were measured. This is an important result of the present work since it demonstrates that melts shorter than a characteristic length (which, here, is calculated to be a little higher than C_{78}) exhibit a strong tendency to fully adsorb on graphite (i.e., with all of their carbons along the chain backbone).

The reason why trains of 4 and 5 bonds long are not favored is related to the length scale of the first

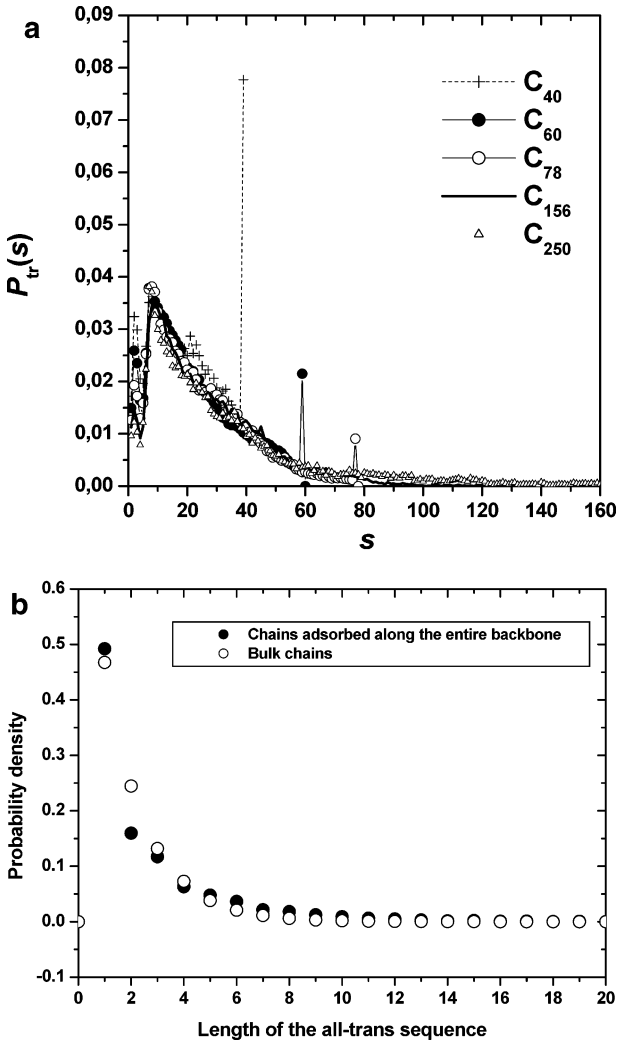

Figure 12. (a) Train size distribution, $P_{tr}(s) = n_{tr}(s)/n_{tr}$, as a function of chain length. (b) Probability density function of torsion angles involved in an all-trans sequence as a function of the size of the all-trans sequence, for C_{78} chains that are adsorbed on the graphite plane along their entire backbone [$T = 450$ K].

adsorption layer (6 Å) and can be understood in terms of the mean train trajectory $\langle z_{tr}(i) \rangle$ discussed above. According to Figure 11a, six C−C bonds are approximately needed to bridge atoms in this layer with carbon atoms in the next adsorption layer and with interior atoms in trains lying 4.0 Å from the graphite plane (i.e., at the minimum of the corresponding potential energy). It takes therefore 6 or 7 C−C bonds for a train to span a length scale equal to twice the gap distance separating atoms at 6 and 4 Å above the graphite. In fact, such an argument suggests that the majority of short trains (with size $s < 6$) must be found at the two ends of the adsorbed chains. We analyzed this by registering the rank numbers of atoms making up trains of a given size or length along the chain. It was indeed found that in the C_{78} melt, for example, 83% of trains of length $s = 2$ bonds and 77% percent of trains of length $s = 4$ bonds are located at the two chain ends.

Of extreme interest is the probability of encountering trains of length equal to the total chain length; this corresponds to the probability of observing chains whose all skeletal atoms are adsorbed on the graphite plane. Such a probability was found to be extremely high only for the shorter C_{40} melt studied here, manifesting itself

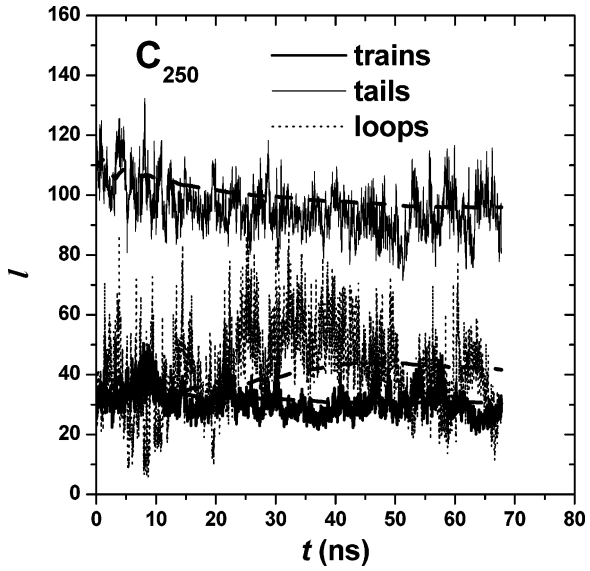

Figure 13. Time evolution of the instantaneous values of the mean length, l, of trains, tails, and loops, as obtained from the MD simulations with the C_{250} PE melt [$T = 450$ K].

in the sharp maximum observed in the $P_{tr}(s)$ curve at $s = 39$, and nonnegligible for the C_{60} and C_{78} systems (see Figure 12a). For the rest of the simulated systems (C_{156}, C_{250}, and C_{400}), the resulting probability was practically zero. The different behavior of the C_{40}, C_{60}, and C_{78} systems should be attributed to their short chain length, for which the energy gained by the adsorption of the entire molecule overrides the strong entropic penalty associated with constraints to chain propagation along the z direction imposed by the solid barrier. At this point, we would like to draw the reader's attention to the following point. It is known that chain confinement can locally promote significant chain ordering characterized by an all-trans sequence of torsion angles even at temperatures a little higher than the polymer crystallization temperature; this phenomenon is known in the literature as surface-induced crystallization.[57−59] However, all simulations of the present work have been executed at a temperature ($T = 450$ K) significantly higher than the PE crystallization temperature (close to 400 K); consequently, no surface-induced crystallization phenomena must be expected. To verify this, we calculated the percentage or relative population of all-trans sequences in those chains of the C_{78} PE/graphite system that are adsorbed on the graphite plane along their entire backbone; admittedly, if surface-induced crystallization took place, these chains would have been the most likely to crystallize. The results obtained are shown in Figure 12b; also shown in the figure is the corresponding curve obtained from simulations with a bulk C_{78} PE melt system. The similarity of the two curves indicates that, indeed, adsorbed chains (although highly oriented along the graphite plane) do not demonstrate any signs of a crystalline structure.

The average values of the train, loop, and tail size distributions are considered in Figures 13 and 14. Figure 13 presents the time evolution of the instantaneous and running average values of the average train, tail, and loop length from the MD simulation with the C_{250} PE/graphite system. At thermodynamic equilibrium, it is seen that, for this system, $l_{tr} \approx 30$, $l_l \approx 50$, and $l_t \approx 95$. The dependence of the mean train length, l_{tr}, mean loop length, l_l, and mean tail length, l_t, on chain

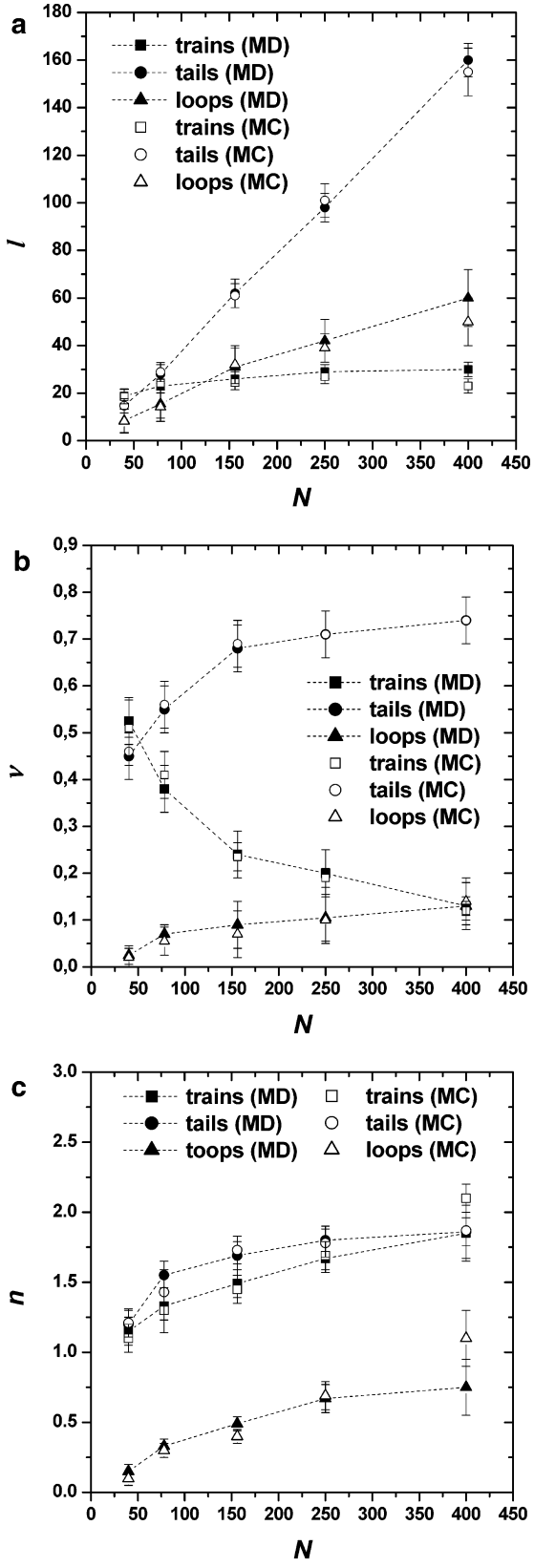

Figure 14. (a) Average length of trains, l_{tr}, loops, l_l, and tails, l_t, as a function of chain length. (b) Average fraction of segments belonging to adsorbed chains found in trains, ν_{tr}, loops, ν_l, and tails, ν_t, as a function of chain length. (c) Average number of trains, n_{tr}, loops, n_l, and tails, n_t, per adsorbed chain [$T = 450$ K].

length, N, is reported in Figure 14a. Two sets of data are shown in the figure corresponding to the two independent simulations with the MC and MD algorithms, respectively, for each system. Our simulation predictions for the chain length dependence of l_{tr}, l_l, and l_t can be directly compared against the results of the Scheutjens−Fleer theory in the limit of zero solvent concentration. Figure 14a shows that, with increasing chain length, l_{tr} tends to a plateau or constant value, equal to about 30 C−C bonds. Taking into account that roughly 12 carbon atoms of our PE melt atomistic model correspond to 1 Kuhn segment, this limiting value for the average train length corresponds to 2.5 Kuhn segments, as opposed to the value of 3.4 reported by Scheutjens−Fleer. As far as the chain length dependence of the average loop size is concerned, Figure 14a shows it to increase monotonically with increasing chain length, which also agrees with the results of the Scheutjens−Fleer lattice theory. Of interest is the variation of the average tail size with chain length, for which the Scheutjens−Fleer theory predicts a strictly linear dependence, with a slope equal to 0.34. Our atomistic simulation results, albeit restricted to low molecular weight PE liquids, also predict a linear dependence of l_t on N, with a slope (extracted from the simulation results with the longer C_{156}, C_{250}, and C_{400} systems) approximately equal to 0.39 ± 0.03.

Figure 14b gives the average fraction of C−C bonds in trains, ν_{tr}, loops, ν_l, and tails, ν_t. With increasing chain length, ν_l and ν_t increase monotonically, approaching constant values in the limit of long molecular weight melts; in contrast, ν_{tr} decreases monotonically tending to zero in the limit of high molecular weight melts. The curves in Figure 14b show also that, in contrast to the long chain length limit where tails dominate the adsorbed amount, in short chain melts both tails and trains contribute significantly (practically equally) to the conformation of the adsorbed layer, taking nearly all bonds. For the shortest C_{40} chain length system simulated here, for example, trains and tails take about 95% of the total number of adsorbed C−C bonds. Most of these results have been predicted by the Scheutjens−Fleer lattice statistical theory;[6] however, it is important to notice that our atomistic simulations predict a sharper transition from the short-chain to the long-chain (or true polymeric) adsorption limit than the Scheutjens−Fleer lattice theory.

Figure 14c gives the average number of trains, n_{tr}, loops, n, and tails, n_t, per adsorbed chain, and their dependence on chain length. The large error bars in the data of the figure obtained from the MC simulations reflect the computational difficulties encountered in equilibrating the train and loop structures of the adsorbed layer with our double-bridging algorithm, due to the fact that certain moves (such as the end-bridging and the generalized reptation) or chain/chain recombinations in the double-bridging algorithm that lead to polydispersity have been completely disallowed in order to keep the simulated samples strictly monodisperse (and eliminate any tendency for segregation of the longer species on the graphite surface).[57] In fact, the MD method was seen to be more effective in equilibrating the average number of these fine polymer conformations at the graphite interface than the monodisperse chain version of the double-bridging MC algorithm. As a result, the data of Figure 14c that are more representative of the true structure of the adsorbed layer are those of the MD rather than of the MC method. In agreement with the Scheutjens−Fleer lattice model, Figure 14c demonstrates that n_{tr}, n_l, and n_t increase

monotonically with increasing chain length (of course, n_t should never exceed the value of 2). For example, the average number of tails per chain changes from 1.2 in the adsorbed C_{40} melt to 1.8 in the adsorbed C_{250} melt. The reader can also observe that, again, the transition from the short-chain to the long-chain (or true polymeric) adsorption limit in Figure 14c is sharper than what is predicted by the Scheutjens−Fleer lattice theory. Extending the present atomistic simulation efforts to longer PE melts, such as C_{500} and C_{1000}, and investigating the scaling laws quantifying the power law dependence of the tail, train, and loop statistics (segment fraction and average number per chain) on chain length will be the subject of a future contribution.

V. Conclusions

We have presented results from an atomistic modeling approach to the simulation of the interface between a polymer melt and a crystalline solid substrate. As a test case, a thin film of PE melt supported by a semiinfinite graphite substrate on the one side and exposed to vacuum on the other has been simulated. The simulation was carried out by following a hierarchical modeling strategy consisting of four steps: (a) generation of an initial structure for the confined PE melt film, (b) minimization of its total (the sum of polymer/polymer, polymer/graphite, and polymer/vacuum) potential energy with respect to all microscopic degrees of freedom, (c) thorough thermal equilibration of its short- and long-length scale structural and conformational characteristics in the vicinity of the two interfaces with an efficient MC algorithm involving state-of-the-art chain connectivity-altering moves, and (d) execution of long MD simulations for times up to 100 ns to monitor the diffusive motion of segments and of entire chains in the two interfacial regions and probe its anisotropy.

Local structural and conformational features at the two interfaces were analyzed at the level of both individual atoms or bonds and entire chains. The local mass density near the graphite plane exhibits an oscillatory profile characteristic of a system adsorbed on the solid surface in multiple layers. At least three such adsorption layers can be identified in the present atomistic simulations. Chain conformations are pronouncedly flattened in the first adsorption layer, gradually assuming their bulk characteristics as one moves away from the solid, over a distance roughly equal to the unperturbed chain end-to-end length. As one moves from one adsorption layer to the next, sudden alterations are observed in the dihedral angle distribution, with successive torsion angles alternating abruptly between trans and gauche states, and vice versa, over length scales less than 15 Å from the graphite plane. These alterations have been explained in terms of bonds belonging to the interior of trains preferring long sequences of all-trans conformations and of bonds bridging atoms in adjacent adsorption layers.

At the melt free surface, on the other hand, the local mass density falls monotonically from its bulk value to zero along the characteristic sigmoidal shape. The length scale over which density changes are observed at the free surface depends on the molecular weight of the melt. Skeletal bonds tend to orient parallel to the free surface.

The structure of the adsorbed layer on graphite has further been analyzed in terms of the distribution of adsorbed segments in trains, loops, and tails. The statistics of trains, loops, and tails (size distributions, average lengths, and segment fractions) have been analyzed in detail and compared exhaustively with the predictions of the Scheutjens−Fleer theory for homopolymer adsorption from solution, in the limit of zero solvent concentration.

The purpose of the present paper has been to explore volumetric, structural, and conformational aspects of the PE melt/graphite and PE melt/vacuum interfaces. Dynamic aspects of the simulated PE systems at the two interfaces are discussed in the next paper.

Acknowledgment. We are grateful to the European Community project PMILS (Polymer Modelling at Integrated time and Length Scales), Contract No. G5RD-CT-2002-00720, for financial support in the course of this work. Very fruitful discussions with Professors D. Theodorou, G. Fleer, F. Leermakers, A. Beris, and S. Kumar are deeply acknowledged.

Appendix. Calculation of the Tail Correction to the Polymer/Polymer Interatomic Interaction Potential and Its Incorporation in Atomistic MC and MD Simulations of Nonuniform Density Profile Systems

The derivation of the long-range contribution to the nonbonded interatomic interaction potential in molecular mechanics (MM) and molecular dynamics (MD) approaches to nonuniform density polymer systems has been discussed in detail by Mansfield and Theodorou in their work on the simulation of (a) the interface between amorphous glassy atactic polypropylene and a graphite basal plane[20] and (b) the free surface of amorphous glassy atactic polypropylene.[21] Mansfield and Theodorou state that failure to properly account for the long tail correction to the potential energy in simulations of semiinfinite systems, where density may vary relatively abruptly across the simulation box, can lead to an artificial imbalance between cohesive and adhesive interactions, causing the latter to appear too strong. The method is extended here to simulations carried out with the technique of MC and is generalized to account for the fact that, in a MC simulation, a relatively small number of atom coordinates is changed every time a move is attempted.

We consider an atom pair ij in the simulation box and its contribution to the long-range correction in the potential energy, V_{ij}^{tails}. This should be the sum of contributions from the nonbonded interactions of atom i with atom j and all its images; the long-range interactions of atom i with its own images should also be taken into account. Consequently

$$V_{ij}^{\text{tails}} = \sum_{m \in \{\text{images of } j\}} (V_{i,m}^{\text{LJ}} - V_{i,m}^{\text{trunc}}) \qquad \text{(A.1)}$$

where $V_{i,m}^{\text{LJ}}$ denotes the full LJ interaction potential and $V_{i,m}^{\text{trunc}}$ its spherically truncated form (see eq 2 in the main text). The total tail contribution to the polymer/polymer cohesive energy is found by summing over all atoms i and all atoms j:

$$V_{\text{tails}} = \sum_{i=1}^{n}\sum_{j=1}^{n}\sum_{m\in\{\text{images of } j\}}\frac{1}{2}(V_{i,m}^{\text{LJ}} - V_{i,m}^{\text{trunc}}) \quad \text{(A.2)}$$

where n is the total number of atoms in the simulation box, and the factor $^1/_2$ takes care of double counting the interactions.

The summations in eq A.1 can be carried out by "smearing" all m images of atom j (including the minimum image) parallel to the xy plane (where the periodic boundary conditions apply) within a slice of thickness δ. This allows treating discrete images as a continuum space variable with atomic density equal to $1/(L_xL_y\delta)$, where L_x and L_y are the lengths of the simulation box in the x and y directions, in the space of a parallelepiped with infinite dimensions along x and y and equal to δ along z. This allows one to cast eq A.1 in the following form:

$$V_{i,m}^{\text{tails}} = \int_{z_j}^{z_j+\delta}\mathrm{d}z\int_{\rho}^{\infty}r\,\mathrm{d}r\int_0^{2\pi}\mathrm{d}\varphi\,\frac{1}{L_xL_y\delta}V^{\text{LJ}}[\sqrt{r^2+(z-z_i)^2}]$$

$$\rho = \sqrt{\max\{R_c^{\,2} - (z-z_i)^2, 0\}} \quad \text{(A.3)}$$

The simulation box is subsequently partitioned into N_b thin layers (bins) along the z direction, each of thickness δ; the number of united atoms in each such layer is denoted as $N(z_j)$, j=1, 2, ..., N_b. Substituting eq A.3 into eq A.2, and taking advantage of the symmetry with respect to polar angle φ, leads to the following expression for the total truncation energy:

$$V^{\text{tails}} = \sum_{i=1}^{n}\frac{1}{2}\sum_{J_{\text{layer}}=0}^{N_b-1}2\pi N(J_{\text{layer}})\times \int_{J_{\text{layer}}\delta}^{(J_{\text{layer}}+1)\delta}\mathrm{d}z\int_{\rho}^{\infty}r\,\mathrm{d}r\,\frac{1}{L_xL_y\delta}V^{\text{LJ}}[\sqrt{r^2+(z-z_i)^2}]$$

$$\approx \sum_{i=1}^{n}\frac{1}{2}\sum_{J_{\text{layer}}=0}^{N_b-1}2\pi N(J_{\text{layer}})\times \int_{\rho}^{\infty}r\,\mathrm{d}r\,\frac{1}{L_xL_y}V^{\text{LJ}}[\sqrt{r^2+(J_{\text{layer}}\delta - z_i)^2}]$$

$$\rho = \sqrt{\max\{R_c^{\,2} - (J_{\text{layer}}\delta - z_i)^2, 0\}} \quad \text{(A.4)}$$

By substituting the exact functional form for the LJ potential in eq A.4, we obtain

$$V^{\text{tails}} = \sum_{i=1}^{n}\sum_{J_{\text{layer}}=0}^{N_b-1}\frac{\pi N(J_{\text{layer}})}{L_xL_y}\epsilon\left(\frac{2}{5}\frac{\sigma^{12}}{r_1^{\,10}} - \frac{\sigma^6}{r_1^{\,4}}\right)$$

$$r_1^{\,2} = \max\{R_c^{\,2} - (J_{\text{layer}}\delta - z_i)^2, 0\} + (J_{\text{layer}}\delta - z_i)^2 \quad \text{(A.5)}$$

Equation A.5 is the starting point for the calculation of the tail correction in an MD or MC simulation. In an MD simulation, for example, a correction to the force on atom i of the form $\mathbf{F}^i = (F_x^i, F_y^i, F_z^i)$ whose components are obtained by differentiating the second sum in eq A.5 with respect to x_i, y_i, z_i:

$$F_z^i = \begin{cases} 0 & |J_{\text{layer}}\delta - z_i| \le R_c \\ 4\epsilon\displaystyle\sum_{J_{\text{layer}}=0}^{N_b-1}\frac{\pi N(J_{\text{layer}})}{L_xL_y}\left(\frac{\sigma^6}{(J_{\text{layer}}\delta - z_i)^5} - \frac{\sigma^{12}}{(J_{\text{layer}}\delta - z_i)^{11}}\right) & |J_{\text{layer}}\delta - z_i| > R_c \end{cases} \quad \text{(A.6)}$$

$$F_y^i = F_x^i = 0$$

should be incorporated before we integrate the equations of motion.

The calculation of the tail correction to the force through eq A.6 assumes that the function $N(J_{\text{layer}})$ is known; this requires a do-loop over all atoms in the system. Such a calculation can significantly delay the execution of the MD simulation; however, one can make use of a list which, similar to the Verlet list, can be updated every time an atom moves a distance greater than a prescribed distance, $\delta_{\max}$; here, this was chosen equal to half the bin thickness δ. A value of 1.54 Å was used for the latter throughout the present simulations.

In a MC simulation, eq A.5 had better be used in the following form:

$$V^{\text{tails}} = \sum_{I_{\text{layer}}=0}^{N_b-1}N(I_{\text{layer}})\sum_{J_{\text{layer}}=0}^{N_b-1}\frac{\pi N(J_{\text{layer}})}{L_xL_y}\epsilon\left(\frac{2}{5}\frac{\sigma^{12}}{r_1^{\,10}} - \frac{\sigma^6}{r_1^{\,4}}\right)$$

$$r_1^{\,2} = \max\{R_c^{\,2} - (J_{\text{layer}}\delta - I_{\text{layer}}\delta)^2, 0\} + (J_{\text{layer}}\delta - I_{\text{layer}}\delta)^2 \quad \text{(A.7)}$$

In the course of the MC simulation, extreme care should be taken of the fact that, in an attempted move, the z coordinate of some or all of the atoms involved in the move can change by so much that they may have to be relocated in a different layer. Relocating moved atoms to different layers changes the atomic density profile, $N(z)$, which, in turn, affects the value of the tail correction to the system potential energy and, consequently, the potential energy difference between "old" and "new" states needed in the evaluation of the Metropolis criterion for the acceptance of the move; to properly account for this, one needs to know the atomic density profile, $N(z)$, in the new system configuration. Such an operation can also affect the performance or efficiency of the algorithm. To go around this problem, we note that, in an attempted MC move, only a limited number of atoms participate; thus, one must care only for a finite number of entries in the list $N(z)$ that may be affected by the move. In fact, if n_{moved} is the total number of atoms involved in the MC move, then it is only $2n_{\text{moved}}$ layers at most whose population must be reevaluated during the move (the "old" and the "new" layers/positions of the moved atoms).

MC calculations can further be accelerated by realizing that, in the calculation of ΔV^{tail} through eq A.7, there is no need to execute the complete double do-loop over all layers (or bins) which scales as N_b^2 with the number of bins, N_b. If i_1, i_2, ..., i_m, $0 \le m \le 2n_{\text{moved}}$, are the indices of the bins whose populations are affected by the attempted MC move, the double sum in the calculation of the total tail correction in eq A.7 can be regrouped as follows:

$$V^{\text{tails}} = \sum_{\substack{I_{\text{layer}}=0 \\ I_{\text{layer}} \notin \{i_1,i_2,\ldots,i_m\}}}^{N_b-1} N(I_{\text{layer}}) \sum_{\substack{J_{\text{layer}}=0 \\ J_{\text{layer}} \notin \{i_1,i_2,\ldots,i_m\}}}^{N_b-1} \frac{\pi N(J_{\text{layer}})}{L_x L_y} \epsilon\left(\frac{2}{5}\frac{\sigma^{12}}{r_1^{10}} - \frac{\sigma^6}{r_1^4}\right) +$$
$$\sum_{\substack{I_{\text{layer}}=0 \\ I_{\text{layer}} \in \{i_1,i_2,\ldots,i_m\}}}^{N_b-1} N(I_{\text{layer}}) \sum_{\substack{J_{\text{layer}}=0 \\ J_{\text{layer}} \notin \{i_1,i_2,\ldots,i_m\}}}^{N_b-1} \frac{\pi N(J_{\text{layer}})}{L_x L_y} \epsilon\left(\frac{2}{5}\frac{\sigma^{12}}{r_1^{10}} - \frac{\sigma^6}{r_1^4}\right) +$$
$$\sum_{\substack{I_{\text{layer}}=0 \\ I_{\text{layer}} \notin \{i_1,i_2,\ldots,i_m\}}}^{N_b-1} N(I_{\text{layer}}) \sum_{\substack{J_{\text{layer}}=0 \\ J_{\text{layer}} \in \{i_1,i_2,\ldots,i_m\}}}^{N_b-1} \frac{\pi N(J_{\text{layer}})}{L_x L_y} \epsilon\left(\frac{2}{5}\frac{\sigma^{12}}{r_1^{10}} - \frac{\sigma^6}{r_1^4}\right) +$$
$$\sum_{\substack{I_{\text{layer}}=0 \\ I_{\text{layer}} \in \{i_1,i_2,\ldots,i_m\}}}^{N_b-1} N(I_{\text{layer}}) \sum_{\substack{J_{\text{layer}}=0 \\ J_{\text{layer}} \in \{i_1,i_2,\ldots,i_m\}}}^{N_b-1} \frac{\pi N(J_{\text{layer}})}{L_x L_y} \epsilon\left(\frac{2}{5}\frac{\sigma^{12}}{r_1^{10}} - \frac{\sigma^6}{r_1^4}\right) \quad \text{(A.8)}$$

$$r_1^2 = \max\{R_c^2 - (J_{\text{layer}}\delta - I_{\text{layer}}\delta)^2, 0\} + (J_{\text{layer}}\delta - I_{\text{layer}}\delta)^2$$

This happens because when we subtract $V_{\text{old}}^{\text{tail}}$ from $V_{\text{new}}^{\text{tail}}$ to calculate ΔV^{tail}, the first term in eq A.8 corresponding to bins whose population needs not be updated cancels out. The calculation of the total tail correction, $(N_b - 1)2n_{\text{moved}}$, can therefore be cast in the form of a double do-loop of size equal just $(N_b - 1)2n_{\text{moved}}$. As far as the choice of the parameter δ is concerned, consistently with the strategy followed in our MD simulations, a value equal to 1.54 Å was used throughout the present MC simulations. [Trial runs with smaller δ values gave identical simulation results.]

References and Notes

(1) Wu, S. *Polymer Interface and Adhesion*; Marcel Dekker: New York, 1982.
(2) Kinloch, A. J. *Adhesion and Adhesives: Science and Technology*; Chapman and Hall: New York, 1987.
(3) Fleer, G. J.; Cohen Stuart, M. A.; Scheutjens, J. M. H. M.; Cosgrove, T.; Vincent, B. *Polymers at Interfaces*; Chapman & Hall: London, 1993.
(4) Ramamurthy, A. V. *J. Rheol.* **1986**, *30*, 337.
(5) De Gennes, P. G. *Macromolecules* **1981**, *14*, 1637.
(6) Scheutjens, J. M. H. M.; Fleer, G. J. *J. Phys. Chem.* **1979**, *83*, 1619; **1980**, *84*, 178.
(7) Semenov, A. N.; Bonet-Avalos, J.; Johner, A.; Joanny, J. F. *Macromolecules* **1996**, *29*, 2179.
(8) Semenov, A. N.; Joanny, J. F. *J. Phys. II* **1995**, *5*, 859.
(9) Johner, A.; Bonet-Avalos, J.; Van der Linden, C. C.; Semenov, A. N.; Joanny, J. F. *Macromolecules* **1996**, *29*, 3629.
(10) Wang, Y.; Rajagopalan, R. *J. Chem. Phys.* **1996**, *105*, 696.
(11) Fleer, G. J.; Van Male, J.; Johner, A. *Macromolecules* **1999**, *32*, 825.
(12) Fleer, G. J.; Van Male, J.; Johner, A. *Macromolecules* **1999**, *32*, 845.
(13) Joannis, J.; Park, C. W.; Thomatos, J.; Bitsanis, I. A. *Langmuir* **2001**, *17*, 69.
(14) Mavrantzas, V. G.; Beris, A. N. *J. Chem. Phys.* **1999**, *110*, 616, 628.
(15) Theodorou, D. N. *Macromolecules* **1988**, *21*, 1400; **1989**, *22*, 4578; **1989**, *22*, 4589.
(16) Sanchez, I. C.; Lacombe, R. H. *J. Phys. Chem.* **1976**, *80*, 2352.
(17) Sanchez, I. C. *J. Colloid Interface Sci.* **1979**, *69*, 539.
(18) Mansfield, K. F.; Theodorou, D. N. *Macromolecules* **1989**, *22*, 3143.
(19) Mansfield, K. F.; Theodorou, D. N. *Macromolecules* **1990**, *23*, 4430.
(20) Mansfield, K. F.; Theodorou, D. N. *Macromolecules* **1991**, *24*, 4295.
(21) Mansfield, K. F.; Theodorou, D. N. *Macromolecules* **1991**, *24*, 6283.
(22) Bareman, J. P.; Cardini, G.; Klein, M. L. *Phys. Rev. Lett.* **1988**, *60*, 2152.
(23) Xia, T. K.; Ouyang, J.; Ribarsky, M. W.; Landman, U. *Phys. Rev. Lett.* **1992**, *69*, 1967.
(24) Kumar, S. K.; Vacatello, M.; Yoon, D. Y. *Macromolecules* **1990**, *23*, 2189.
(25) Matsuda, T.; Smith, G. D.; Winkler, R. G.; Yoon, D. Y. *Macromolecules* **1995**, *28*, 165.
(26) Winkler, R. G.; Matsuda, T.; Yoon, D. Y. *J. Chem. Phys.* **1993**, *98*, 731.
(27) Clancy, T. C.; Mattice, W. L. *Comput. Theor. Polym. Sci.* **1999**, *9*, 261.
(28) Milchev, A.; Binder, K. *J. Chem. Phys.* **2001**, *114*, 8610.
(29) Mischler, P. C.; Baschnagel, J.; Dasgupta, S.; Binder, K. *Polymer* **2002**, *43*, 467.
(30) Hansen, F. Y.; Herwig, K. W.; Matthies, B.; Taub, H. *Phys. Rev. Lett.* **1999**, *83*, 2362.
(31) Borodin, O.; Smith, G. D.; Bandyopadhyaya, R.; Byutner, O. *Macromolecules* **2003**, *36*, 7873.
(32) Delle Site, L.; Abrams, C. F.; Alavi, A.; Kremer, K. *Phys. Rev. Lett.* **2002**, *89*, 156103.
(33) Delle Site, L.; Salvatore, L.; Kremer, K. *J. Am. Chem. Soc.* **2004**, *126*, 2944.
(34) Harmandaris, V. A.; Mavrantzas, V. G. Molecular Dynamics Simulation of Polymers. In *Simulation Methods for Modeling Polymers*; Theodorou, D. N., Kotelyanskii, M. J., Eds.; Marcel Dekker: New York, 2004.
(35) Mavrantzas, V. G. Monte Carlo Simulation of Chain Molecules. In *Handbook of Materials Modeling. Volume I: Methods and Models*; Yip, S., Ed.; Springer: Dordrecht, The Netherlands, 2005; pp 1−15.
(36) Theodorou, D. N. Variable-connectivity Monte Carlo algorithms for the atomistic simulation of long-chain polymer systems. In Nielaba P., Mareschal, M., Ciccotti, G., Eds.; *Bridging Time Scales: Molecular Simulations for the Next Decade*; Springer-Verlag: Berlin, 2002.
(37) Mavrantzas, V. G.; Boone, T. D.; Zervopoulou, E.; Theodorou, D. N. *Macromolecules* **1999**, *32*, 5072.
(38) Karayiannis, N. C.; Mavrantzas, V. G.; Theodorou, D. N. *Phys. Rev. Lett.* **2002**, *88*, 105503. Karayiannis, N. C.; Giannousaki, A. E.; Mavrantzas, V. G.; Theodorou, D. N. *J. Chem. Phys.* **2002**, *117*, 5465.
(39) Martin, M. G.; Siepmann, J. I. *J. Phys. Chem. B* **1998**, *102*, 2569.
(40) Trokhymchuk, A.; Alejandre, J. *J. Chem. Phys.* **1999**, *111*, 8510.
(41) Van der Ploeg, P.; Berendsen, H. J. *J. Chem. Phys.* **1982**, *76*, 3271.
(42) Toxvaerd, S. *J. Chem. Phys.* **1997**, *107*, 5197.
(43) Steele, W. A. *Surf. Sci.* **1973**, *36*, 317.
(44) Theodorou, D. N.; Suter, U. W. *Macromolecules* **1985**, *18*, 1847.
(45) Allen, M. P.; Tildesley, D. J. *Computer Simulation of Liquids*; Claredon Press: Oxford, 1986.
(46) Ryckaert, J. P.; Ciccoti, G.; Berendsen, H. J. C. *J. Comput. Phys.* **1977**, *101*, 327.
(47) Andersen, H. C. *J. Comput. Phys.* **1983**, *52*, 24.
(48) Martyna, G. J.; Tuckerman, M. E.; Tobias, D. J.; Klein, M. L. *Mol. Phys.* **1996**, *87*, 1117.
(49) Yoon, D. Y.; Vacatello, M.; Smith, G. D. In *Monte Carlo and Molecular Dynamics Simulations in Polymer Science*; Binder, K., Ed.; Oxford University Press: New York, 1995.
(50) Wu, D. T.; Fredrickson, G. H.; Carton, J. P.; Ajdari, A.; Leibler, L. *J. Polym. Sci., Part B: Polym. Phys.* **1995**, *33*, 2373.

(51) Jones, R. L.; Kumar, Ho. D. L.; Brider, R. M.; Russel, T. P. *Nature (London)* **1999**, *400*, 146.
(52) Kumar, S. K.; Vacatello, M.; Yoon, D. Y. *Macromolecules* **1989**, *22*, 4589.
(53) Bitsanis, I. A.; Brinke, G. *J. Chem. Phys.* **1993**, *99*, 3100.
(54) Zannoni, C. In *The Molecular Pohysics of Liquid Crystals*; Luckhurst, G. R., Gray, G. W., Eds.; Academic: New York, 1979.
(55) Fischel, L. B.; Theodorou, D. N. *J. Chem. Soc., Faraday Trans.* **1995**, *91*, 2381.
(56) Mavrantzas, V. G.; Theodorou, D. N. *Macromolecules* **1998**, *31*, 7934.
(57) Xu, G.; Mattice, W. L. *J. Chem. Phys.* **2002**, *117*, 3440.
(58) Doye, J. P. K.; Frenkel, D. *J. Chem. Phys.* **1998**, *109*, 10033.
(59) Waheed, N.; Lavine, M. S.; Rutledge, G. C. *J. Chem. Phys.* **2002**, *116*, 2301.

MA050176R